Acoustic monitoring of the tide height and slope-water intrusion at the New Jersey Shelf in winter conditions

Altan Turgut,[a] Marshall Orr, and Bruce Pasewark[b]
Naval Research Laboratory, Acoustics Division, Washington, DC 20375

(Received 21 June 2006; revised 5 February 2007; accepted 9 February 2007)

Waveguide invariant theory is used to describe the frequency shifts of constant acoustic intensity level curves in broadband signal spectrograms measured at the New Jersey Shelf during the winter of 2003. The broadband signals (270–330 Hz) were transmitted from a fixed source and received at three fixed receivers, located at 10, 20, and 30 km range along a cross-shelf propagation track. The constant acoustic intensity level curves of the received signals indicate regular frequency shifts that can be well predicted by the change in water depth observed through tens of tidal cycles. A second pattern of frequency shifts is observed at only 30 km range where significant variability of slope-water intrusion was measured. An excellent agreement between observed frequency shifts of the constant acoustic intensity levels and those predicted by the change in tide height and slope water elevations suggests the capability of long-term acoustic monitoring of tide and slope water intrusions in winter conditions. © *2007 Acoustical Society of America.* [DOI: 10.1121/1.2713705]

PACS number(s): 43.30.Bp, 43.30.Pc, 43.30.Re [RAS] Pages: 2534–2541

I. INTRODUCTION

In a shallow-water waveguide, pressure spectra of acoustic signals generated by distant broadband sources often exhibit striation patterns when plotted in time (or range) due to constructive and destructive interference of propagating acoustic modes. For a range-independent waveguide, Chuprov[1] derived a simple formula for the so-called *waveguide invariant* that characterizes the dispersive nature of the waveguide and relates the observed slope of the striations to range and frequency. The range-frequency waveguide invariant, usually designated as beta, has the canonical value of one for an isovelocity waveguide with perfectly reflecting bottom. However, for an arbitrary sound-speed profile, different combinations of modes at different frequencies provide slightly different values of beta. Effects of time- and range-varying waveguide parameters on the striation patterns have also been studied.[2–6] Weston *et al.*[2] observed a change in the frequency-time interference patterns of broadband (4.1–4.5 kHz) signals that could be explained by the dependency of mode parameters on water depth that changed through the tidal cycle. They derived a simple formula for the slope of the interference patterns by using the expression for the modal interaction distance, and showed that measured slopes of interference patterns agree well with the theoretical predictions. Grachev[3] used a unified waveguide invariant theory and showed that the range-frequency invariant beta and several time-frequency waveguide invariant parameters could be used to estimate the slope of constant acoustic intensity levels for more complicated waveguides. Recently, Petkinov and Kuzkin[4] summarized the previously reported theoretical estimations of the frequency shift of constant acoustic intensity, levels produced by tides, internal waves, surface waves, and diurnal oscillations of frontal zone.

Several previous experimental data showed evidence of tidal height effects on the acoustic intensity striation patterns with partial success.[2,7,8] However, acoustic monitoring of a single oceanographic process was never envisioned due to the complexity of environmental conditions in shallow water. Our high-quality experimental data show that some of these oceanographic processes can be isolated and monitored by low-frequency acoustic propagation measurements conducted under winter conditions. In addition to tidal height monitoring, the effects of slope-water intrusion on the measured acoustic intensity striation patterns is demonstrated for the first time by using the same data set collected at the Middle Atlantic Bight. Slope-water intrusion and climatology of shelf break fronts in the Middle Atlantic Bight have been reported based on extensive historical data[9] and most recent oceanographic data from the New England shelf break PRIMER experiment.[10] During the PRIMER experiment, an integrated study of acoustics and oceanography was conducted to understand low-frequency acoustic propagation in the presence of a shelf-break front both in winter and summer conditions.[11] Their oceanographic measurements indicated that dynamics of the shelf break front is strongly influenced by external forcing of Gulf Stream rings and filaments, causing temporal correlation scales of temperature and salinity to be about 1.3 days.[10,12] They also noted a warm near-bottom slope, water layer at the floor of the shelf break front extending shoreward to the 100 m isobath that is also affected by the strong external forcing. Based on numerical simulations, they showed that measured sound-speed fields, representing the dynamics of shelf break fronts, can cause significant acoustic field variability.[11] Our experiment, Relationship between Array Gain and Shelf-break fluid processes (RAGS), was conducted on the outer New Jersey Shelf to further study the interaction of sound with shelf-break fluid processes during winter conditions. The oceanographic data from the RAGS experiment also revealed a warm near-bottom slope-water layer extending shoreward between 80

[a]Electronic mail: turgut@wave.nrl.navy.mil
[b]Deceased.

 0001-4966/2007/121(5)/2534/8/$23.00

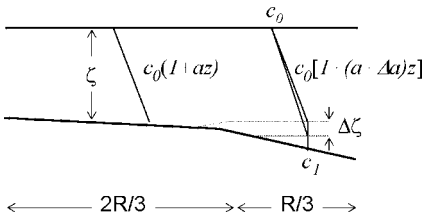

FIG. 1. A simplified RAGS03 experiment acoustic propagation environment representing both ideal waveguide and surface channel propagation conditions.

and 100 m isobaths with about 20 m change in layer thickness within the time scales of one to two days. Observed frequency-time interference patterns of broadband (270–330 Hz) signals showed direct evidence of the effects of these near-bottom slope-water intrusions on low-frequency acoustic propagation.

In the present paper, waveguide invariant theory is used to explain the observed frequency shift of the constant acoustic intensity levels of broadband signals by variations in tide height and thickness of the near-bottom slope water. Acoustic monitoring of the near-bottom slope-water intrusion is demonstrated. In Sec. II, derivations of both range-frequency and time-frequency waveguide invariants are given for a simple waveguide with range- and time-dependent parameters. In Sec. III, numerical simulations are used to investigate the applicability of analytically derived waveguide invariants to the RAGS03 data. In Sec. IV, the RAGS03 New Jersey Shelf experiment is briefly described and observed time-frequency patterns are compared with the theoretical predictions. A summary and discussion are given in Sec. V.

II. THEORY

In this section, we derive various waveguide invariant parameters to describe the observed frequency shift of the constant acoustic intensity levels during the RAGS03 experiment. We first consider the case where the observable is the acoustic intensity from a distant source measured as a function of range and frequency. We derive a specific form of the waveguide invariant that makes explicit its dependence on the propagating acoustic modes. We also consider the case where the source and receiver are fixed in space and the observed acoustic intensity is varied in time due to the time-dependent properties of waveguide. For later use on data from the RAGS03 experiment, we then outline various waveguide invariant parameters for an ideal waveguide and a surface channel (see Fig. 1).

The acoustic intensity, when mapped versus range and frequency, often exhibits a pattern of striations that represent level curves. To analyze the properties of the level curves, let I be the observed intensity as a function of range r from the source and frequency ω. The level curves satisfy

$$\frac{\partial I}{d\omega}d\omega+\frac{\partial I}{\partial r}dr=0. \tag{1}$$

Solving for the slope $d\omega/dr$ of the striations yields

$$\frac{\partial\omega}{dr}=-\frac{\partial I/\partial r}{\partial I/\partial\omega}. \tag{2}$$

To analyze Eq. (2), it is convenient to use a normal mode representation for the intensity. For source and receiver depths z_s, and z, respectively, the associated pressure p in the far field can be approximated as

$$p=\sum_m(\xi_m r)^{-1/2}\Psi_m(z_s)\Psi_m(z)e^{i(\xi_m+i\alpha_m)r}, \tag{3}$$

where Ψ_m are the mode functions and ξ_m the corresponding horizontal wave numbers. The modal attenuation α_m accounts for bottom loss. Certain unimportant scaling terms have been suppressed. It follows that the intensity, $I=|p|^2$, is

$$I=\sum_{m,n}A_{mn}\exp(i\Delta\xi_{mn}r), \tag{4}$$

where $\Delta\xi_{mn}$ are horizontal wave number differences between modes n and m. The amplitudes A_{mn} can be derived from Eq. (3). Neglecting the weak range and frequency dependence in A_{mn}, the derivatives can be calculated

$$\frac{\partial I}{\partial r}\approx i\omega\sum_{m,n}A_{mn}\frac{\Delta\xi_{mn}}{\omega}\exp(i\Delta\xi_{mn}r), \tag{5a}$$

$$\frac{\partial I}{\partial\omega}\approx ir\sum_{m,n}A_{mn}\frac{\partial\Delta\xi_{mn}}{\partial\omega}\exp(i\Delta\xi_{mn}r), \tag{5b}$$

where $\Delta\xi_{mn}/\omega$ are the phase slowness differences with modal phase velocity $v=(\xi/\omega)^{-1}$ and $\partial\Delta\xi_{mn}/\partial\omega$ are the mode group slowness differences with modal group velocity $u=(\partial\xi/\partial\omega)^{-1}$.

Brekhovskikh and Lysanov[5] give a definition for the waveguide invariant as a derivative of the phase slowness with respect to the group slowness. For a group of closely spaced modes, the derivative of the phase slowness with respect to the group slowness is assumed to be independent of mode order and frequency, and represented by a scalar parameter as[1]

$$\beta=-\frac{\Delta(1/v)}{\Delta(1/u)}=-\frac{\Delta\xi_{mn}/\omega}{\partial\Delta\xi_{mn}/\partial\omega}. \tag{6}$$

Equation (6) can be used in Eq. (5a) to eliminate the term related to the phase slowness difference. Combining Eqs. (2)–(6) yields for the slope of the striations

$$\frac{d\omega}{dr}=\beta\frac{\omega}{r}. \tag{7}$$

Grachev[3] noted that in addition to the above-mentioned range-frequency waveguide invariant, other acoustic field (time-frequency) invariants can be derived for a waveguide with time-dependent parameters, such as waveguide thickness and propagation speed. In this case, similar to Eq. (2), slope of the intensity striations yields

$$\frac{d\omega}{d\eta}=-\frac{\partial I/\partial\eta}{\partial I/\partial\omega}, \tag{8}$$

where η is a time-varying waveguide parameter. Using the normal mode representation of intensity and following a

derivation similar to Eqs. (3)–(6), a time-frequency waveguide invariant γ can be defined as

$$\gamma = -\frac{\frac{\partial \Delta\xi_{mn}}{\partial \eta}/\omega}{\frac{\partial \Delta\xi_{mn}}{\partial \omega}/\eta}, \tag{9}$$

from which the slope of the intensity striations can be calculated as

$$\frac{d\omega}{d\eta} = \gamma\frac{\omega}{\eta}. \tag{10}$$

Simultaneous solution of differential equations (7) and (9) for $\Delta\xi_{mn}$ yields[3]

$$\Delta\xi_{mn} = C_{mn}\eta^{\gamma/\beta}\omega^{-1/\beta}, \tag{11}$$

where C_{mn} is a constant that depends only on the mode order.

For an ideal waveguide with an isovelocity sound speed profile, the horizontal component of the wave number is given by[5] $\xi_m=[(\omega/c)^2-(\pi m/h)^2]^{1/2}$, from which an approximate form of the horizontal wave number difference can be calculated as $\Delta\xi_{mn}\cong\pi^2(m^2-n^2)(c/2\omega h^2)$. Using the approximate horizontal wave number difference in the above equation yields the values $\beta=1$ for the range-frequency waveguide invariant, $\gamma_h=-2$ for the time-frequency waveguide invariant of waveguide thickness, and $\gamma_c=1$ for the time-frequency waveguide invariant of sound speed. In this case, the frequency shift of level curves due to a change in water depth can be calculated from Eq. (10) by setting $\gamma=h$ as

$$\frac{\Delta\omega}{\omega} = -\frac{2\Delta h}{h}. \tag{12}$$

The above-presented formula was first derived by Weston *et al.*[2] by considering the dependence of modal interaction distance on the water depth. He then used the above-noted formula to explain the observed slopes of the interference patterns during a half tidal cycle.

For a surface channel with a linear variation in the square index of refraction, $n^2(z)=c_0^2/c^2(z)=1-az$, the horizontal wave number differences in Eq. (11) is given as

$$\Delta\xi_{mn} \approx \tfrac{1}{2}(y_m - y_n)a^{2/3}c_0^{1/3}\omega^{-1/3}, \tag{13}$$

where y_m and y_n are the roots of the Airy function. Equation (13) yields the values $\beta=-3$ for the range-frequency waveguide invariant, $\gamma_a=-2$ for the time-frequency waveguide invariant of the sound-speed gradient, and $\gamma_{c_0}=1$ for the time-frequency waveguide invariant of the sound speed. In the case where $a\ll 1$, assuming a linear variation in the index of refraction, the sound speed profile can be approximated as $c(z)\approx c_0(1+az/2)$.

Calculations of horizontal wave number differences can be found in Kibblewhite and Denham[13] for an upward refracting surface channel or in Kuzkin[14] for a downward refracting near-bottom channel in the form

$$\Delta\xi_{mn} \approx \frac{(3\pi)^{2/3}}{2}[(m-3/4)^{2/3}-(n-3/4)^{2/3}]a^{2/3}c_0^{1/3}\omega^{-1/3}. \tag{14}$$

Equation (14) also yields the values $\beta=-3$ for the range-frequency waveguide invariant, $\gamma_a=-2$ for the time-frequency waveguide invariant of the sound-speed gradient, and $\gamma_{c_0}=1$ for the time-frequency waveguide invariant of the sound speed. Let us consider a surface channel with thickness ζ, surface sound speed c_0, and sound speed gradient a overlaying a bottom layer with a constant sound speed c_1 (see Fig. 1 for the region $2R/3<r<R$ where R is the distance between the fixed source and receiver). We assume that both refracting modes (trapped in the surface channel) and reflecting modes (bottom/surface) exist in the waveguide. For trapped modes, using sound speed gradient $a=(c_1-c_0)/c_0\zeta$ and its variation $\Delta a=-\Delta\zeta(c_1-c_0)/c_0\zeta^2$, the time-frequency waveguide invariant for surface duct thickness can be related to the time-frequency waveguide invariant for sound-speed gradient as $\gamma_\zeta=-\gamma_a$. In this case, the frequency shift due to a change in surface duct thickness can be calculated from Eq. (14) as

$$\frac{\Delta\omega}{\omega} = \frac{2\Delta a}{2} = -\frac{2\Delta\zeta}{\zeta}. \tag{15}$$

For the (bottom/surface) reflecting modes, Eq. (12) can also be used to calculate the frequency shift due to change in water depth. Note that in the case of gradual range dependency of the waveguide as shown in Fig. 1. Equation (9) can be extended as[6]

$$\gamma(r) = -\frac{\int_0^r \frac{\partial \Delta\xi_{mn}}{\partial \eta}dr/\omega}{\int_0^r \frac{\partial \Delta\xi_{mn}}{\partial \omega}dr/\eta}. \tag{16}$$

For the (bottom/surface) reflecting modes at ranges $0<r<2R/3$, the frequency shift can be calculated from Eq. (16) as[6]

$$\frac{\Delta\omega}{\omega} = -\frac{2\Delta h}{h_{\text{eff}}}, \tag{17}$$

where $h_{\text{eff}}=(h_s h_r)^{1/2}$ is the effective water depth,[15] h_s is the water depth at the source, and h_r is the water depth at the receiver. Due to slope-water intrusion, if the surface waveguide thickness ζ is temporally varied only at ranges $2R/3<r<R$ as shown in Fig. 1, the frequency shift due to a change in surface duct thickness can be calculated from Eq. (16) as

$$\frac{\Delta\omega}{\omega} = -\frac{2\Delta\zeta}{3\zeta}. \tag{18}$$

III. NUMERICAL SIMULATIONS

In this section, acoustic intensity patterns are calculated numerically for the propagation environment depicted in Fig. 1. Waveguide invariants derived in Sec. II are compared with

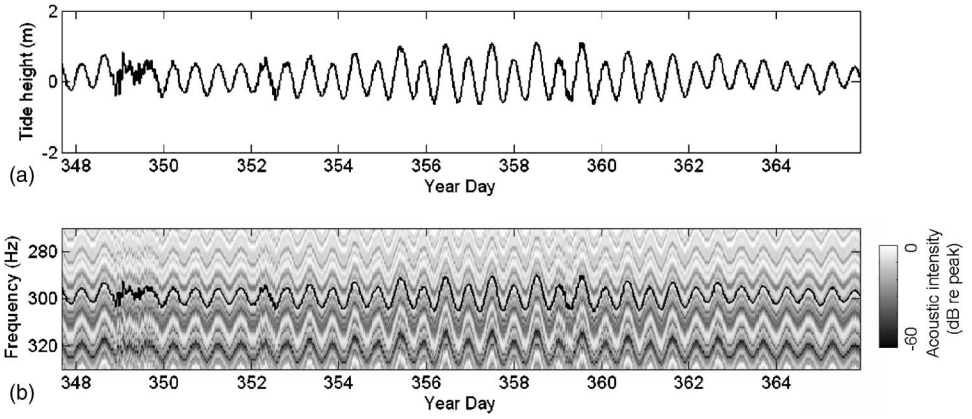

FIG. 2. (a) Measured tide height at 20 km range and (b) simulated acoustic intensity levels using the measured tide during the period from YD348 to YD365. The frequency shifts predicted by using Eq. (17) is also shown (solid line).

those calculated from the simulated data. Numerical simulations are performed using a broadband adiabatic normal-mode propagation model that uses the modal eigenvalues and eigenfunctions generated by the numerical code FEMODE.[16] First, frequency shifts of 270–330 Hz signals are simulated at 20 km range by changing the water depth according to the measured tidal information during the period from YD347 to YD365 (see Fig. 2). The source is located 19 m above the bottom in 65 m water depth. The water depth is linearly increased with range so that the water depth at the receiver (20 km range) is 89 m. Sound speed profiles in the water column are described in Fig. 1 within the region $0<r<2R/3$ where $c_0=1484$ m/s at the surface and $c_1=1502$ at 60 m depth. Throughout the calculations, the same bottom sound-speed profiles and attenuation values were used. The bottom sound speed is described as $c_b=1580$ m/s at the seafloor and 1680 m/s at 20 mbsf (meters-below-seafloor) and 1890 m/s at 50 mbsf and below. A value of 0.1 dB per wavelength was used for the bottom attenuation coefficient.

Figure 2(a) shows measured tidal variation of the water depth at 20 km propagation range. Figure 2(b) shows calculated acoustic intensity levels at a receiver located at 20 km range and 20 m depth for the period from YD347 to YD365. The frequency shifts due to measured tidal height variations are also calculated for the frequency $f=300$ Hz by using Eq. (17) and plotted in Fig. 2(b) (thick solid line). Note the excellent agreement between the simulated frequency shifts and those calculated by using Eq. (17). According to Eq. (17), if the effective water depth is $h_{\text{eff}}=(h_s h_r)^{1/2}=76$ m, and typical tidal height variation is $\Delta h=0.75$ m, a frequency shift of $\Delta f=6$ Hz is expected at the frequency $f=300$ Hz. This frequency shift can be easily measured with high resolution as is shown in Fig. 2(b) confirming the feasibility of acoustic monitoring of tide height on the continental shelves.

As a second case, dependency of the frequency shifts on the near-bottom (slope-water) layer thickness variations is analyzed by numerical simulations. The same environmental parameters were used as in the previous case, except that the thickness of the surface channel is changed in time according to values extracted from measured temperature profiles at 20 km range [see Fig. 3(a)]. Figure 3(b) shows the calculated acoustic intensity levels at a receiver located at 30 km range and 25 m depth for the period from YD347 to YD365. The frequency shifts due to measured changes in the thickness of the surface layer (or near-bottom slope water layer) are also calculated for the frequency $f=300$ Hz by using Eq. (18) and plotted in Fig. 3(a) (thick solid line). There is an excellent agreement between the simulated frequency shifts and those calculated by using Eq. (18). According to Eq. (18), if the mean thickness of the surface layer is $\zeta=85$ m and the thickness variation is $\Delta\zeta=20$ m, a frequency shift of $\Delta f=23.5$ Hz is expected at the frequency $f=300$ Hz. This frequency shift is easily measured with high resolution, as is shown in Fig. 3(b), confirming the feasibility of acoustic monitoring of the change in the thickness of near-bottom slope water. In Fig. 3(a), the change in surface channel thickness exceeds 25 m during several time periods (e.g., at YD361). One would need to use acoustic signals with bandwidths larger than 60 Hz to monitor these extreme cases.

Next, the depth variation of the range-frequency waveguide invariant beta is analyzed to isolate the effects of re-

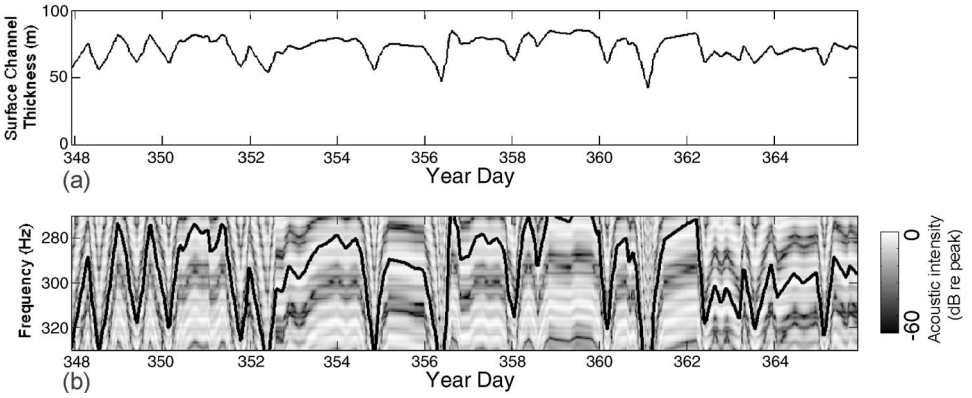

FIG. 3. (a) Surface channel thickness extracted from measured temperature profiles and (b) simulated acoustic intensity levels using the measured tide during the period from YD348 to YD365. The frequency shifts predicted by using Eq. (18) are also shown (solid line).

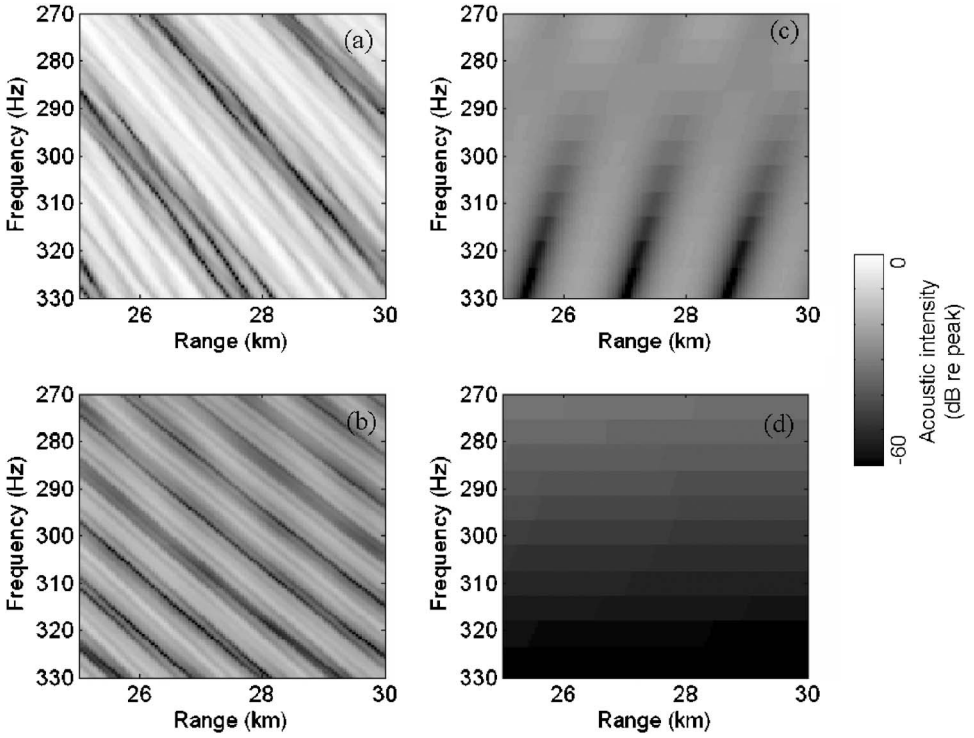

FIG. 4. Simulated acoustic intensity levels for a source moving from 25 to 30 km range using (a), (b) all propagating modes and (b), (d) the first two modes only. (a), (c) Receiver in the surface channel (at 25 m). (b), (d) Receiver below the surface channel (at 95 m).

flecting and refracting modes in a waveguide having both an upward refracting surface channel and an isovelocity near-bottom layer (the region $2R/3 < r < R$ in Fig. 1). Figure 4(a) shows the calculated acoustic intensity levels for a receiver at 25 m depth as the source moved from 25 to 30 km range. The complexity of the acoustic intensity striation patterns indicates that interference of more than one group of acoustic modes might be involved. Figure 4(b) shows the calculated spectral levels for a receiver at 95 m depth. In this case, the acoustic intensity striation patterns are much more regular and the interference of only one group of modes is dominant. For this case, using $r=27.5$ km, $\Delta r=5$ km, $f=300$ Hz, and $\Delta f=55$ Hz, Eq. (7) yields a value of $\beta \approx 1$ for the range-frequency waveguide parameter. Figures 4(c) and 4(d) show the calculated spectral levels at 25 and 95 m depths that use the first two modes only. In Fig. 4(d), the contribution of the first two modes to the total received levels [see Fig. 4(b)] is minor for the receiver at 95 m depth. Nonexistence of the striation patterns indicates that the relative contribution from one of the first two modes is much weaker than the other. In Fig. 4(c) the slopes of the acoustic intensity striations are reversed for the receiver at 25 m depth with respect to the total field case [Fig. 4(a)] indicating the existence of a group of low-order acoustic modes that are trapped in the surface channel. For this case, using $r=29$ km, $\Delta r=1.9$ km, $f=300$ Hz, and $\Delta f=-60$ Hz, Eq. (7) yields a value of $\beta \approx -3$ for the range-frequency waveguide parameter.

IV. EXPERIMENTAL RESULTS

The Relationship between Array Gain and Shelf-break fluid processes (RAGS) experiment was conducted on the New Jersey Shelf between 12 December 2003 and 4 January 2004. The primary objective was to study the interaction of sound with shelf-break fluid processes in the ocean waveguide. The collection of high-quality acoustic and oceanographic data provided new analysis and interesting findings in additional research areas.[17,18] In this paper, a unique observation of the frequency shifts of the constant acoustic intensity level curves and their relation to tidal height and slope-water intrusion are explained by using the waveguide invariant theory. The experiment featured moored sources transmitting 16, 60, and 100 Hz bandwidth acoustic signals at respective center frequencies of 224, 300, and 500 Hz. Three vertical receiving arrays, each having 32 elements, were located at ranges 10, 20, and 30 km from the sources (see Fig. 5). Only the 300 Hz signals with 60 Hz bandwidth are considered in this paper. Figures 6(a)–6(c) show the acoustic intensity levels measured at 30 m depth at 10, 20, and 30 km range, respectively. The regular sinusoidal inter-

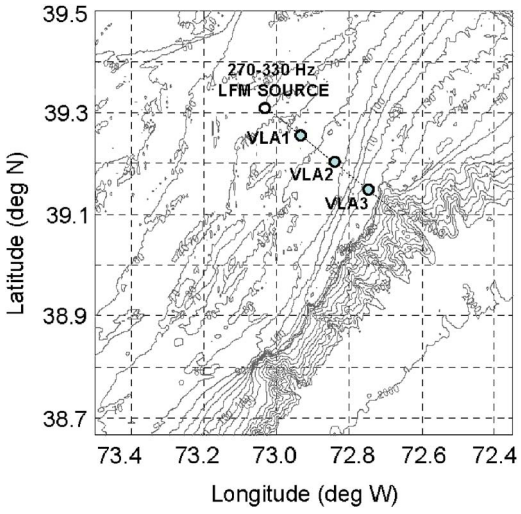

FIG. 5. (Color online) RAGS03 experimental area and source/receiver configuration.

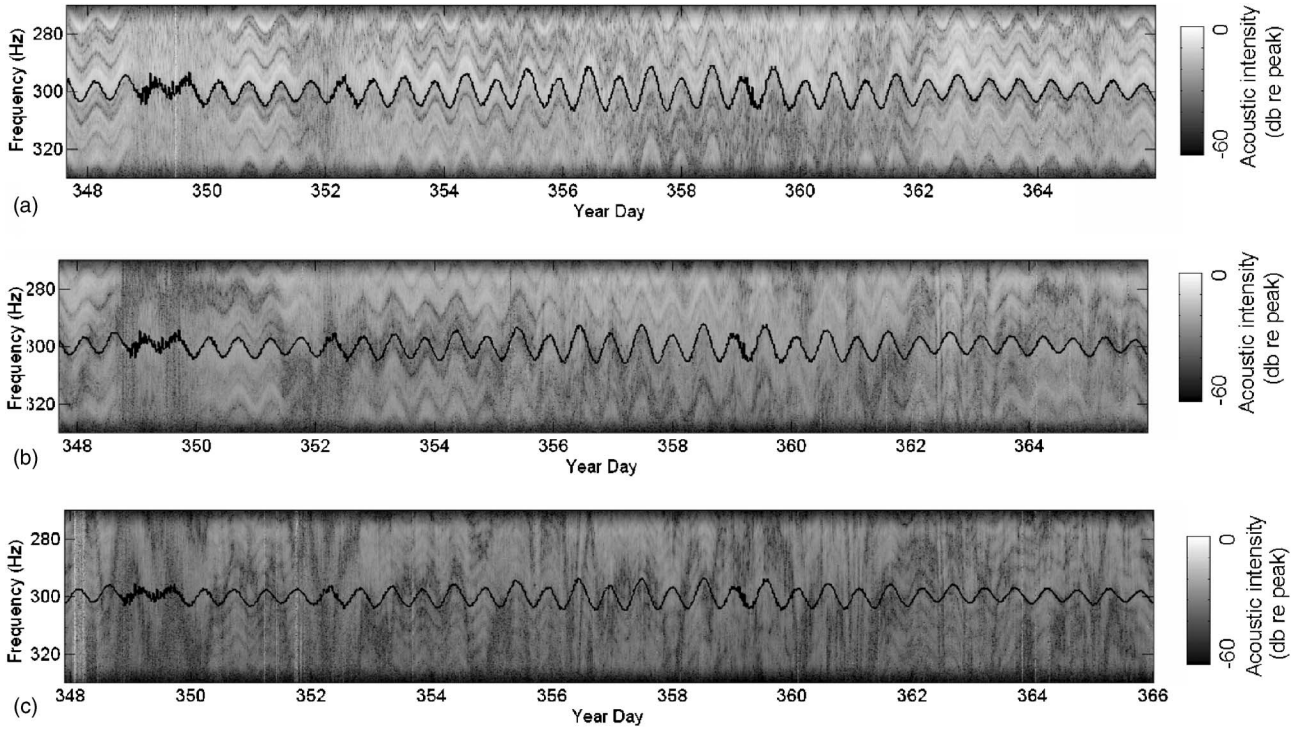

FIG. 6. Measured acoustic intensity levels at (a) 10 km, (b) 20 km, and (c) 30 km range. Corresponding frequency shifts predicted by using Eq. (17) are also shown (solid lines).

ference patterns can be observed throughout the experimental period from YD347 to YD365. The interference patterns slightly deteriorate due to an increase in the range-dependency of waveguide for larger receiver distances. Also, as the effective depth increases with range, the amplitude of the sinusoidal patterns becomes smaller for more distant receivers. The frequency shifts due to the measured tidal height variations [see Fig. 2(b)] are calculated by using the corresponding effective depths 67, 76, and 91 m in Eq. (17) and are also plotted in Figs. 6(a)–6(c) (solid line), respectively. Figures 6(a) and 6(b) show an excellent agreement between the measured acoustic intensity level curves and those calculated by using Eq. (17). Conversely, this also indicates that one can monitor tidal height variation from the measured acoustic intensity level curves. Figure 6(c) shows that acoustic intensity striation patterns are much more complex at 30 km range and the direct effects of tidal height variations can be seen only during certain periods (e.g., at YD350, YD353, and YD361). This indicates significant contributions from the variability of waveguide parameters other than that of tidal height. Figure 6(c) also depicts a second pattern of much larger frequency shifts that can be related to the near-bottom slope water intrusion. Details of the RAGS03 oceanographic measurements are described next to demonstrate the effects of slope water intrusion on the measured frequency shifts of acoustic intensity level curves.

The hydrographic measurements during the RAGS03 experiment include thermistor chains located at each VLA and several days of towed CTD surveys along the acoustic propagation tracks. Figures 7(a) and 7(b) show two towed CTD casts along the acoustic propagation track taken on YD345 and YD347. The near-bottom slope water intrusion extends shoreward from the 100 m isobath to the 80 m isobath within two days. Also the 1500 m/s isospeed contour is elevated about 30 m, indicating an increase of near-bottom slope water layer thickness. In Fig. 7(c), representative sound speed profiles, plotted at 22 km range, depict an upward refracting surface channel and an isospeed near-bottom layer. Unfortunately, towed CTD casts were limited to only a few days so that monitoring of slope water intrusion for the entire experiment duration was not possible by towed CTD surveys. However, thermistor chains at each VLA provided point measurements of temperature fields that were used to predict the extent of the slope water intrusion from YD437 to YD365.

Figure 8(a) shows the measured temperature field at VLA2 (20 km range) depicting an increase in the warm near-bottom layer thickness, mainly due to the external forcing of the shelf break front by Gulf Stream eddies and filaments. Figure 8(b) shows the acoustic intensity levels measured at VLA3 (30 km range) and 30 m depth. The solid line in Fig. 8(a) is manually traced at a maximum temperature gradient to depict the magnitude of change in the near-bottom layer thickness. The frequency shifts due to the measured near-bottom layer thickness are calculated by using Eq. (18) and are also plotted in Fig. 8(b). For the duration of the entire experiment, an excellent agreement has been observed between the measured acoustic intensity level curves and those estimated by using Eq. (18). This reveals the long-term monitoring capability of the near-bottom layer thickness from the acoustic intensity level curves measured during winter conditions.

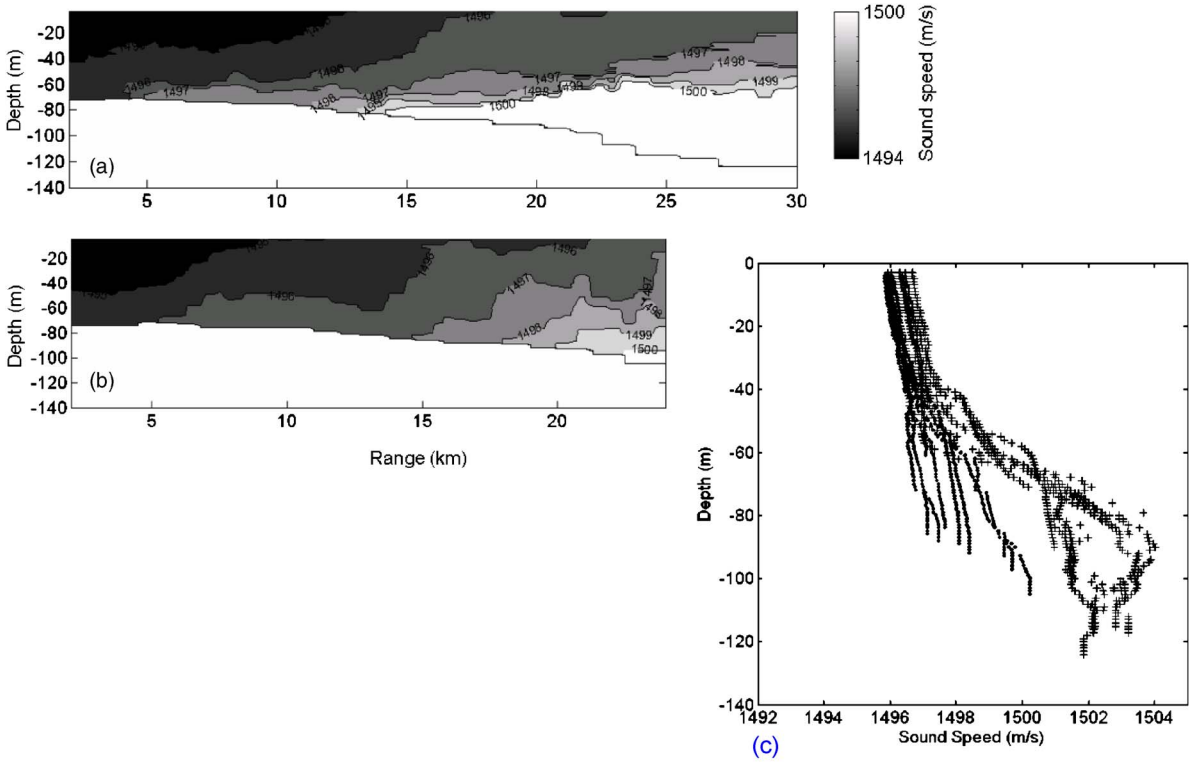

FIG. 7. (Color online) Sound speed fields along the acoustic propagation track extracted from SeaSoar casts taken on (a) YD345, (b) YD347, and (c) representative sound speed profiles near 22 km range.

V. SUMMARY

The relationship between changes in tide height and slopes of acoustic intensity level curves has been reported previously[2,12] with very limited experimental data. In this paper, we have demonstrated the robustness and reliability of this relationship by the high-quality measurements of the tide height and acoustic intensity level curves for much longer durations (tens of tidal cycles) during winter conditions. Also, we have shown the direct effects of slope-water intrusion on the frequency shifts of acoustic intensity level curves. The theoretical predictions, given in Sec. II, provide an accurate estimation of the frequency variation of acoustic intensity level curves from the variations of tidal height and near-bottom layer thickness measured in the Middle Atlantic Bight. The excellent agreement between measured frequency shifts of intensity level curves and those by predicted from measured tide height and near-bottom layer thickness indicates the feasibility of long-term acoustic monitoring of tide

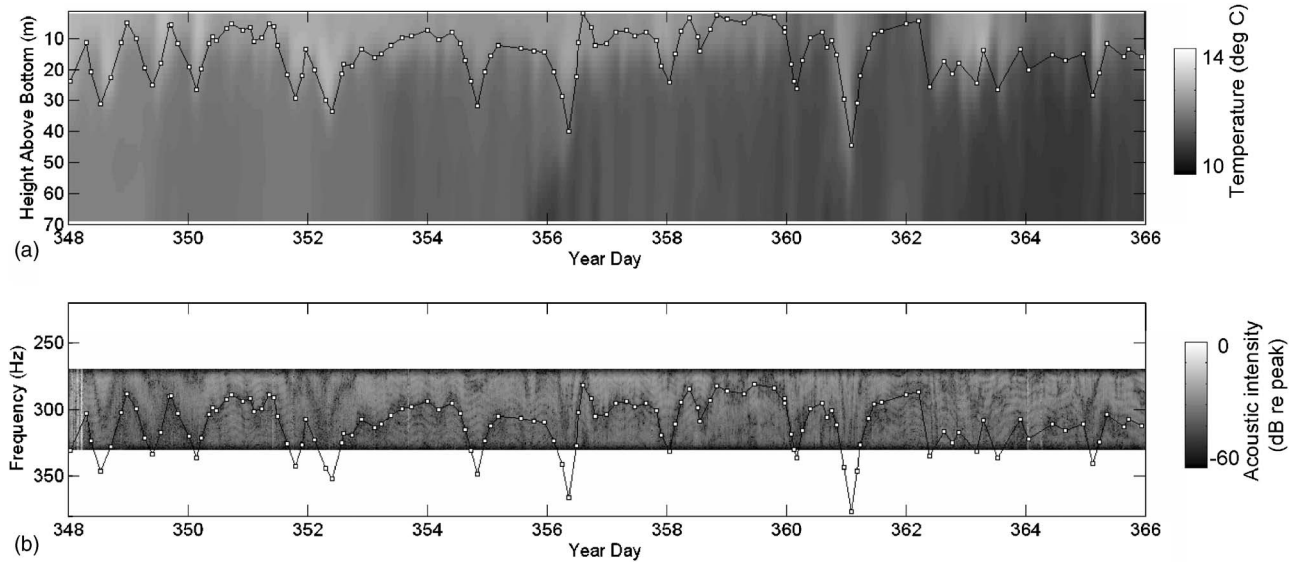

FIG. 8. (a) Measured temperature field at 20 km range and manually traced maximum temperature gradient (solid line), (b) acoustic intensity levels measured at 30 km range and 30 m depth. The frequency shifts predicted by using Eq. (18) are also shown (solid line).

height and near-bottom slope water intrusion in the Middle Atlantic Bight under winter conditions. A natural extension of our results would be the estimation of the effective depth of the acoustic propagation track from the tidal height data obtained from oceanographic measurements or tide prediction models. The effective depth is one of the inverted parameters in the geoacoustic inversion methods commonly used in shallow water.[15] Another potential application of our results is that a smoothly varying two-dimensional (2D) bathymetry can be mapped and monitored by means of an acoustic tomography experiment by collecting broadband acoustic propagation data. Analysis of the 2D mapping capability of the bathymetry and slope-water intrusion is beyond the scope of this paper and results of a low-cost tomography experiment are planned to be reported in the near feature.

ACKNOWLEDGMENTS

This work was supported by the Office of Naval Research. We thank Peter Mignerey David Walsh, Steve Wales, Jeff Schindall, Earl Carey, Michael McCord, and Mark Hulbert of Naval Research Laboratory for their scientific contribution to RAGS experiment. We also thank the captain and crew of the R/V Endeavor and R/V Oceanus for the excellent support throughout the RAGS03 experiment.

[1]S. D. Chuprov, "Interference structure of sound field in the layered ocean," in *Ocean Acoustics. Modern State*, edited by L. M. Brekhovskikh and I. B. Andreeva (Nauka, Moscow, 1982), pp. 71–91.
[2]D. E. Weston, D. Smith, and G. Wearden, "Experiments on time-frequency interference patterns in shallow-water acoustic transmission," J. Sound Vib. **10**, 424–429 (1969).
[3]G. A. Grachev, "Theory of acoustic field invariants in layered waveguides," Acoust. Phys. **39**, 33–35 (1993).
[4]V. G. Petnikov and V. M. Kuz'kin, "Shallow water variability and its manifestation in the interference pattern of sound fields," in *Ocean Acoustic Interference Phenomena and Signal Processing*, edited by W. A. Kuperman and G. L. D'Spain (AIP Conference Proceedings, Melville, NY, 2002), pp. 207–217.
[5]L. M. Brekhovskikh and Y. P. Lysanov, *Fundemantals of Ocean Acoustics*, 2nd ed. (Springer, New York, 1991).
[6]G. L. D'Spain and W. A. Kuperman, "Application of waveguide invariants to analysis of spectograms from shallow water environments that vary in range and azimuth," J. Acoust. Soc. Am. **106**, 2454–2468 (1991).
[7]V. M. Kuz'kin, A. V. Ogurtsov, and V. G. Petkinov, "The effect of hydrodynamic variability on frequency shifts of the interference pattern of a sound field in a shallow sea," Acoust. Phys. **44**, 94–100 (1998).
[8]L. F. Bonder, L. K. Bugeva, and A. N. Rutenko, "Effect of tide on sound propagation in the shelf zone of the Sea of Japan," Acoust. Phys. **46**, 534–543 (2000).
[9]C. A. Linder and G. Gawarkiewicz, "A climatology of the shelfbreak front in the Middle Atlantic Bight," J. Geophys. Res. **103**, 18,405–18,423 (1998).
[10]G. Gawarkiewicz, K. H. Brink, F. Bahr, R. C. Beardsley, M. Caruso, J. F. Lynch, and C.-S. Chui, "A large-amplitude meander of the shelfbreak front during summer south of New England: Observations from the shelfbreak PRIMER experiment," J. Geophys. Res. **109**, 1468–1484 (2004).
[11]J. F. Lynch, A. E. Newhall, B. Sperry, G. Gawarkiewicz, A. Frederics, P. Tyack, C.-S. Chiu, and P. Abbot, "Spatial and temporal variations in acoustic propagation characteristics at the New England shelfbreak front," IEEE J. Ocean. Eng. **28**, 129–150 (2003).
[12]R. S. Pickart, D. J. Torres, T. K. McKee, M. J. Caruso, and J. E. Przystup, "Diagnosing a meander of the shelf break current in the Middle Atlantic Bight," J. Geophys. Res. **104**, 3121–3132 (1999).
[13]A. C. Kibblewhite and R. N. Denham, "Experiment on propagation in surface sound channels," J. Acoust. Soc. Am. **38**, 63–71 (1965).
[14]V. M. Kuz'kin, "Frequency shifts of the sound field interference pattern in a shallow sea," Acoust. Phys. **45**, 224–229 (1999).
[15]C. H. Harrison and M. Siderius, "Effective parameters for matched field geoacoustic inversion in range-dependent environments," IEEE J. Ocean. Eng. **28**, 432–445 (2003).
[16]M. D. Collins, "FEPE user's guide," Naval Ocean Research and Development Activity, Stennis Space Center, MS, NORDA Technical Note No. 365, 1988.
[17]A. Turgut, "Geoacoustic inversion by using broadband ship noise recorded on the New Jersey Shelf," J. Acoust. Soc. Am. **118**, 1857 (2005).
[18]A. Turgut, "Acoustic monitoring of finback whale movements on the New Jersey Shelf," J. Acoust. Soc. Am. **120**, 3266 (2006).